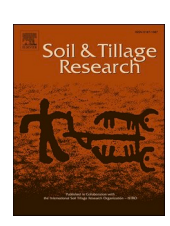
ELSEVIER

Contents lists available at ScienceDirect

### Soil & Tillage Research

journal homepage: www.elsevier.com/locate/still



# Quantifying nutrient loss across particle size fractions in eroded tropical soils using <sup>239+240</sup>Pu fallout radionuclides

Job Isaboke <sup>a,b</sup>, Olivier S. Humphrey <sup>b,\*</sup>, Ruth Njoroge <sup>c</sup>, Odipo Osano <sup>a</sup>, Michael J. Watts <sup>b</sup>

- a Department of Environmental Biology and Health, School of Environmental Studies, University of Eldoret, Eldoret, Kenya
- b Inorganic Geochemistry, Centre for Environmental Geochemistry, British Geological Survey, Nottingham NG12 5GG, UK
- <sup>c</sup> Department of Soil Science, School of Agriculture and Biotechnology, University of Eldoret, Eldoret, Kenya

#### ARTICLE INFO

# Keywords: Plutonium Erosion Land management Particle size Nutrients

#### ABSTRACT

In sub-Saharan Africa, where livelihoods depend on agriculture, steep valley slope cultivation intensifies soil erosion, threatening agricultural sustainability by depleting fertile topsoil of nutrients. This study measured soil erosion and deposition using <sup>239+240</sup>Pu fallout radionuclides and associated macro- and micronutrient loss across particle size fractions in the Oroba Valley, Nandi Hills, Kenya. Three experimental plots were assessed: Plot 1 (conventional tillage) and Plot 2 (terraced agricultural system), both of which were cleared for cultivation in 1940, while Plot 3 (historically shrubland) was recently cleared in 2023. A stratified sampling design was used to collect soil samples, which were analysed for particle size distribution, organic matter (OM) content, pH, and total elemental composition using ICP-MS/MS. The MODERN model to estimate erosion and deposition rates using  $^{239+240}$ Pu inventories integrates nutrient losses across specific particle sizes to estimate the nutrients lost. There was severe soil erosion in Plots 1 and 2, with net losses of 13.68 t ha<sup>-1</sup> yr<sup>-1</sup> and 6.09 t ha<sup>-1</sup> yr<sup>-1</sup>, respectively, while Plot 3 showed minimal loss (0.32 t ha<sup>-1</sup> yr<sup>-1</sup>), reflecting the protective effect of vegetative cover. Fine particles (<100 µm), rich in OM and nutrients (Se, Zn, P, I) were disproportionately lost downslope, particularly in intensively cultivated plots. Terracing in Plot 2 was ineffective due to poor maintenance, with erosion observed at terrace sections. Micronutrient loss, notably Mo, Cu, and Se, was linked to  $<50~\mu m$  particle size erosion, while the large fractions (>100 µm) retained K and Mg. This study shows how <sup>239+240</sup>Pu isotopes can be used as sensitive indicators of soil loss and fertility degradation, offering land management and conservation insights.

#### 1. Introduction

Soil erosion poses a significant ecological threat, displacing approximately 75 billion tonnes of soil annually from terrestrial ecosystems (Walling, 2013; Mabit et al., 2014). This extensive erosion strips away the fertile topsoil essential for agriculture and exacerbates environmental challenges by depositing sediment into riverbeds and reservoirs, thereby degrading the sustainability of water systems (Stocking, 2014; Kathpalia and Bhatla, 2018; Tsegaye, 2019). In Africa, soil erosion is primarily driven by water and wind, with anthropogenic activities substantially accelerating the process (Chi et al., 2019; Zucca et al., 2022). Uncontrolled deforestation and unsustainable agricultural practices are key contributors to soil degradation, particularly in the fragile landscapes of western Kenya (Wanyonyi and Mwangi, 2012; Watene et al., 2021).

In East Africa, soil erosion threatens food security by depleting nutrient-rich topsoil, reducing water retention, and degrading soil structure, thereby impairing fertility and agricultural productivity in a region where farming sustains the majority of livelihoods (Van Straaten, 2002; Gomiero, 2016; Rashmi et al., 2022; Ramteke et al., 2023). By disrupting nutrient distribution, erosion causes deficiencies in essential nutrients required for soil fertility, crop productivity, and plant growth (Karthika et al., 2018; Kathpalia and Bhatla, 2018; Ahmed et al., 2020), with potential downstream effects on the health of primary and secondary consumers. Soil aggregates are broken down by raindrop impact, wind, livestock, or tillage, leaving particles vulnerable to hydraulic or aeolian forces. This accelerates erosion and alters the soil's nutrient equilibrium (Bizmark et al., 2020). Deposited particles accumulate on foot slopes and in aquatic systems, leading to nutrient-rich sediment buildup that promotes eutrophication and disrupts ecosystems. At the

E-mail address: olih@bgs.ac.uk (O.S. Humphrey).

 $<sup>^{\</sup>ast}$  Corresponding author.

source, nutrient depletion weakens soil structure and reduces crop productivity (de Nijs and Cammeraat, 2020; Zhang et al., 2020).

Soil particle fractions strongly influence nutrient retention. Clay, with its large surface area and high cation exchange capacity (CEC), retains nutrients and water but restricts drainage. Silt holds moderate nutrients but is highly erosion-prone, while sand drains rapidly, causing nutrient leaching. During erosion, fine particles and their bound nutrients are easily transported, resulting in fertility decline and reduced crop nutrition (Huang et al., 2020; Saentho et al., 2022; Isaboke et al., 2025).

Tracer-based techniques using <sup>239+240</sup>Pu isotopes provide an effective means to quantify soil erosion and nutrient depletion. By measuring isotope concentrations across soil layers, these tracers allow for a precise assessment of soil displacement, deposition, and nutrient-bound particle movement (Xu et al., 2013; Dowell et al., 2024). Compared to traditional methods,  $^{239+240}$ Pu tracers offer significant advantages, including high sensitivity for detecting small-scale soil movements, long half-lives that enable soil redistribution studies over decades, and the ability to trace micronutrient loss at the particle level (Dowell et al., 2024). Plutonium isotopes ( $^{239+240}$ Pu) were released into the environment mainly through atmospheric nuclear weapons testing in the mid-20th century, particularly between the 1940s and 1960s, before the 1963 Partial Test Ban Treaty (Jinlong et al., 2020; Lukashenko and Edomskaya, 2022). Their long half-lives, 24,100 years for <sup>239</sup>Pu and 6560 years for <sup>240</sup>Pu, combined with resistance to chemical alteration, ensure persistence in soils, sediments, and water for millennia (Croft and Favalli, 2021; Dowell et al., 2023). Although they are environmental contaminants (Schmidt et al., 2012), their global distribution and detectability make them highly valuable tracers for soil erosion and sediment studies, even at locations far from nuclear test sites (Alewell et al., 2017; Dowell et al., 2024). These isotopes have been successfully used to quantify soil loss, sediment transport, and deposition, particularly in areas affected by severe erosion or land use change (Walling, 2013; Mabit et al., 2014; Dowell et al., 2024). Sensitive analytical techniques such as gamma spectrometry enable accurate measurement of isotope concentrations, providing essential data to guide soil conservation and land management strategies (Dowell et al., 2022, 2023).

This study aimed to evaluate the influence of soil erosion on the redistribution of macro- and micronutrients across specific soil particle size fractions under different management practices. The specific objectives were: (1) to employ <sup>239+240</sup>Pu isotopes to quantify soil erosion rates, and (2) to integrate soil erosion rates with particle size distribution data to estimate the redistribution of essential nutrients in field plots.

#### 2. Materials and methods

#### 2.1. Study area

The study was conducted between 2021 and 2023 on three agricultural plots situated on the slopes of Oroba Valley, at Plot 1 (latitude: 0.007735, longitude: 34.987602), Plot 2 (latitude -0.004924, longitude: 35.003758) and Plot 3 (latitude: -0.003332, longitude; 34.989053) in Nandi Hills in a region within the Great Rift Valley, Kenya (Fig. 1). The river Oroba passes through the valley and drains into the Winam Gulf, Lake Victoria. The area falls under the upper highland agroecological zone (Kipkulei et al., 2024) and has bimodal long and short rainfall seasons, with an annual total of 500–1200 mm. The Oroba

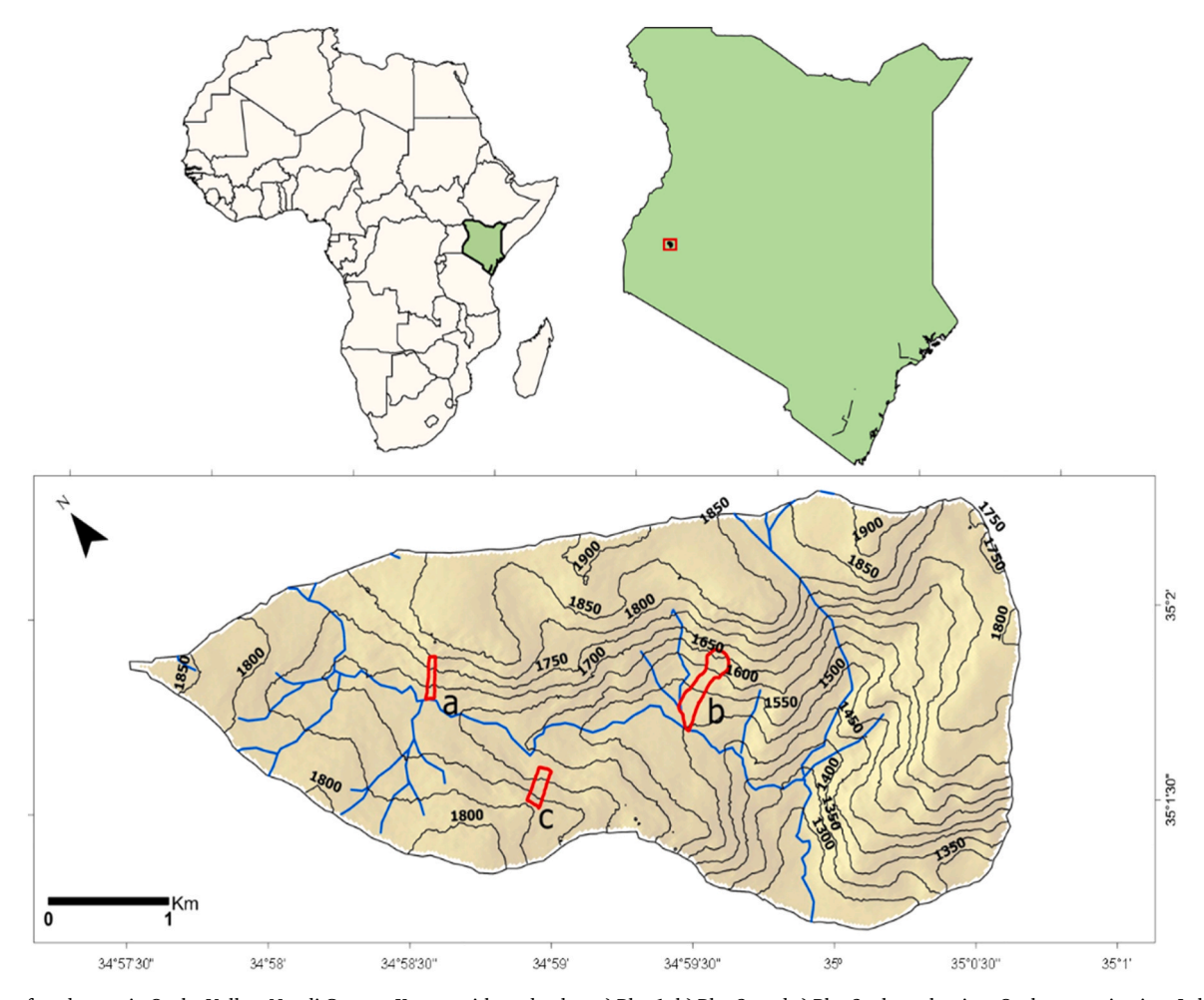


Fig. 1. Map of study area in Oroba Valley, Nandi County, Kenya, with study plots a) Plot 1, b) Plot 2, and c) Plot 3, along the river Oroba emptying into Lake Victoria. The highest (S1) elevation is 1900 m, and the lowest (S5/S6) elevation is 1300 m above sea level.

Valley, situated in a region of western Kenya highly susceptible to erosion, is dominated by subsistence agriculture. Expansion of farmland has accelerated human encroachment into native shrubland and forest ecosystems, reducing vegetation cover and thereby intensifying soil erosion risks (Humphrey et al., 2022)

#### 2.2. Characteristics of the study plots

The three plots were selected due to different farming methods, erosion mitigation methods, and the time since land conversion from natural vegetation to farming. Plots 1 and 2 have been under continuous cultivation for over 80 years since 1940, whereas Plot 3 was recently established and cleared for cultivation in 2023. During the study, this variation provided an opportunity to compare the impact of cultivation duration on soil movement (Montgomery, 2007; Nearing et al., 2017). Plot 1 retained traditional manual-conventional cultivation practices with increased intensities over time, as confirmed by farmers, Plot 2 followed conventional tillage practices, using oxen ploughing and terracing to reduce soil loss, and Plot 3, a shrubland until 2021, is currently halfway conventionally cultivated for maize production (Table 1).

#### 2.3. Sampling design

Using a stratified sampling design based on topography, each of the three plots was subdivided into five or six sections (S1–S5/S6) corresponding to distinct elevation levels (Fig. 2). Within each section, three sampling points were randomly selected. At each point (approximately 1 m  $\times$  1 m), the topsoil (0–20 cm) was collected. A composite sample was prepared at each point by combining soil obtained from three auger flights. Plots 1 and 2 each yielded 15 composite samples (three from each of five sections), while Plot 3 yielded 18 samples (three from each of six sections). All samples were packed in Kraft bags, transported to the Biotechnology Laboratory at the University of Eldoret for drying, disaggregation, and sieving, and were subsequently sent to the British Geological Survey (BGS, Keyworth, Nottingham, UK) for analysis.

#### 2.4. Soil particle size analysis

Particle size fractions were classified within the 0-2 mm range. A 0.22 g portion of air-dried, 2 mm-sieved soil was placed into centrifuge tubes. To oxidise organic matter, 10 mL  $H_2O_2$  was added incrementally to avoid overspill and left for 24 h. Samples were then dried in an  $80^{\circ}$ C water bath. After drying, 20 mL of Calgon solution (50 g of (NaPO<sub>3</sub>)<sub>6</sub> and 7 g of Na<sub>2</sub>CO<sub>3</sub> in 1 L of water) was added, then the samples were shaken for one hour for dispersion. Particle size was measured using an LS 13320 Laser Diffraction Analyser (Beckman Coulter). After analysis, particle sizes were classified into different fractions, similar to Isaboke

**Table 1**Description of three study plots in Oroba Valley in Nandi County, Kenya, of two different sampling sessions.

Plot	Year of sampling	Year of land clearance	Tillage systems	Tillage operation tool	Erosion mitigation measures
Plot	2021	1940	Conventional	Hand-held	None
1	2023		Minimal tillage	Hoe	
Plot	2021	1940	Conventional	Oxen/	Terraces
2	2023			Tractor tillage	
Plot	2021	N/A	No-tillage	N/A	Shrubland
3	2023	2023	Conventional	Hand-held Hoe	None

Conventional tillage- continuous soil disturbances with pulverisation, Minimum tillage-minimal soil disturbance with opening of planting holes only, no-till- no soil disturbance.

et al. (2025) (<10  $\mu$ m, 10  $\mu$ m -25  $\mu$ m, 25  $\mu$ m -50  $\mu$ m, 50  $\mu$ m -100  $\mu$ m, 100  $\mu$ m -500  $\mu$ m, and 500  $\mu$ m -2000  $\mu$ m).

#### 2.5. Soil sample digestion and analysis

Macro and micro-element analysis was conducted on air-dried samples at 40°C and milled. A 0.25 g portion of each soil sample was digested on a programmable hot block using a mixed acid solution (2.5 mL HF, 2 mL HNO<sub>3</sub>, and 2.5 mL H<sub>2</sub>O<sub>2</sub>), following the method described by Joy et al. (2015) and Watts et al. (2020) Iodine extraction used a separate 0.25 g sample with 5 mL 5 % v/v TMAH in a 15 mL Nalgene HDPE bottle. The sample was heated at 70°C for 3 h and then diluted with 5 mL of deionised water. After centrifugation at 3000 rpm for 15 min, the supernatant was analysed. Soil nutrient analysis, samples were analysed by ICP-MS/MS (Agilent 8900 ICP-MS/MS) using helium collision mode for Ca, Mn, Na, Mg, Mo, P, K, Fe, Zn, Cu, and toxic-rare earth elements. Internal standards (Sc, Ge, Rh, In, Te, Ir) corrected signal drift. Iodine was analysed in no-gas mode, with all solutions in 0.5 % TMAH (Watts et al., 2020; Humphrey et al., 2025). The study worked on 12 elements considered nutrients for both plants and animals: 5 Macronutrients, P, Na, Mg, K, and Ca, and 7 micronutrients, I, Se, Cu, Mn, Fe, Zn, and Mo.

#### 2.6. Quantification of organic matter (OM)

Organic matter (OM) was measured using loss-on-ignition (LOI). One gram of the sample was oven-dried at 110°C for 24 h, then ashed at 450°C in a muffle furnace. Organic matter content was calculated from the weight loss following standard LOI procedures (Watts et al., 2020).

#### 2.7. Extraction and analysis of <sup>239+240</sup>Pu activities from soil samples

Fifty grams of finely milled sample were ashed overnight at 550°C to remove OM, then transferred to a PTFE beaker and spiked with 50 pg of <sup>242</sup>Pu tracer for recovery tracking. Isotope leaching was performed by adding 100 mL concentrated HNO₃ and heating at 70°C for 24 h. After centrifugation (3000 rpm, 15 min), the supernatant was filtered through a 0.45  $\mu m$  PTFE filter. The residue was resuspended in 100 mL of distilled water, centrifuged, and filtered. The solution was adjusted to 8 M with HNO<sub>3</sub>, and 4 g NaNO<sub>2</sub> was added to convert Pu to the IV oxidation state. The Pu was isolated using a TEVA resin column, yielding a spike recovery of 81  $\pm$  15 % (Dowell et al., 2023). Calibration used silica sand blanks (20 g) and certified reference material IAEA-384 (0.5 g), achieving detection limits of  $0.108 \pm 0.105$  pg kg<sup>-1</sup> for  $^{239+240}$ Pu and a precision of 114  $\pm$  12 Bq kg $^{-1}$  versus the certified value of  $108\pm13~\text{Bq kg}^{-1}$ . The final quantification of  $^{239+240}\text{Pu}$  was via ICP-MS/MS with O2 gas in collision-reaction mode to resolve the <sup>23</sup> <sup>8</sup>U<sup>1</sup>H<sup>+</sup> interference. Samples were introduced using an Agilent IaS micro-autosampler and Cetac Aridus II desolvating nebuliser. Values below detection were estimated as half the detection limit  $(0.09 \text{ pg kg}^{-1})$ . Plutonium concentrations (pg kg<sup>-1</sup>) were converted to mass activity units using isotope-specific activity (Dowell et al., 2022).

#### 2.8. Quality control

Laboratory quality controls ensured analytical accuracy. Certified reference materials (2711a, BCR-2, BGS 102, GSS-2, and GSS-5) were digested in duplicate with each batch for calibration. The mean recoveries were 93.0  $\pm$  7.7 % (n = 14) for NIST 2711a Montana Soil, 96.0  $\pm$  5.5 % (n = 27) for USGS BCR-2 Basalt, 98.0  $\pm$  8.1 % (n = 15) for BGS 102 Ironstone Soil, and 95.3  $\pm$  7.0 % (n = 8) for NRC MESS-4 Marine Sediment. Triplicate sample analyses in each batch verified repeatability, ensuring data precision and reliability.

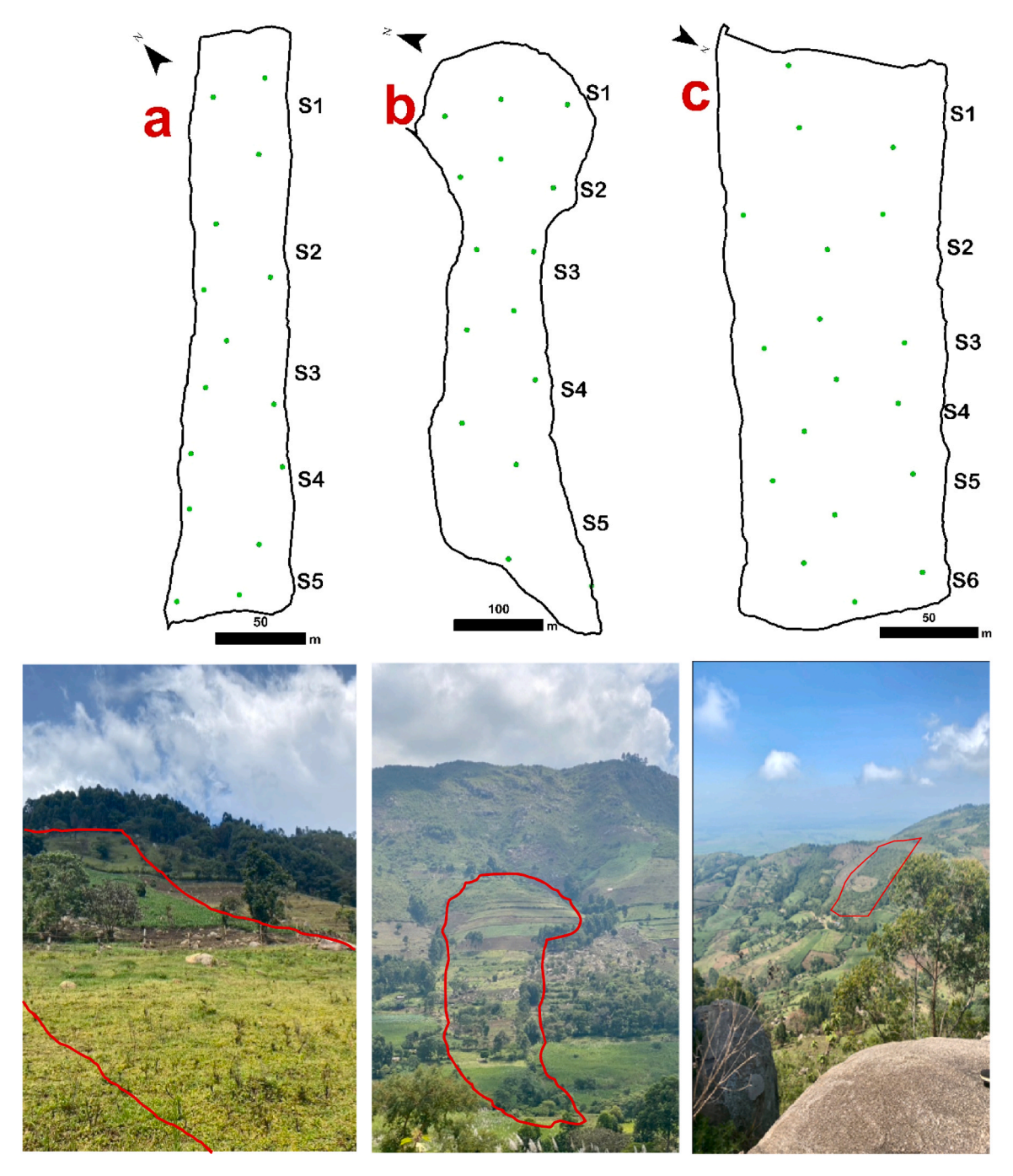


Fig. 2. Spatial layout of the study plots showing demarcated sections and designated sampling points, accompanied by reference photographs of the plots at the initial baseline survey conducted in 2021. Green points indicate the sampling points along each study plot.

#### 2.9. Data analysis

#### 2.9.1. Quantitative model for estimating soil erosion rates

Fallout radionuclide ( $^{239+240}$ Pu) activity, initially measured in Bq kg<sup>-1</sup>, was converted to a real activity (Bq m<sup>-2</sup>) using the < 2 mm soil fraction's mass depth (kg m<sup>-2</sup>). A sum of Pu activities across soil layers served as erosion or deposition indicators. Erosion rates were estimated using the MODERN (Modelling Deposition and Erosion Rates with Radio-Nuclides) model by comparing site-specific inventories to a reference profile, with changes expressed as depth of redistributed soil. MODERN aligns each site's cumulative inventory with the reference to estimate soil loss or gain. For eroded sites (inventory < reference), ten deeper layers were added, extending to 60 cm with exponential FRN decline. For depositional sites (inventory > reference), six surface layers (6 cm) were added to simulate sediment input. Samples exceeding model bounds were excluded (Eq. 1). Assumptions include: (1) Pu originates from global fallout; (2) the reference site reflects baseline <sup>239+240</sup>Pu distribution; and (3) deposition depth matches reference plough depth, enabling land-use-based erosion-deposition analysis (Arata, Alewell, et al., 2016; Arata, Meusburger, et al., 2016; Dowell et al., 2024).

The MODERN Model is expressed as follows:

$$Erosion = 10 \frac{x'xm}{d(t_1 - t_0)} \tag{1}$$

Where erosion in t  $ha^{-1} yr^{-1}$  was calculated as x' is the rate of soil

erosion per depth, xm is the mass depth of the soil at the sample site (kg m<sup>-2</sup>), d is the entire depth increment measured at the sampling site,  $t_1$  is the year of sampling (yr), and  $t_0$  (yr) is the year of the main radionuclide fallout; typically, 1963 for  $^{239+240}$ Pu (Dowell et al., 2024).

#### 2.9.2. Net change soil redistribution

Net change soil distribution indicates changes in soil loss/gain over time, as shown in Eq. 2:

$$NSR = \frac{E - D}{NY(Pu)} \tag{2}$$

Where NSR is the net soil redistribution, E is the total soil loss (erosion: 1963 to the sampling date), D is the total soil gain (deposition: 1963 to sampling date), and NY(Pu) is the number of years since the peak year nuclear bomb was tested near the sampling point (approximately 1963).

#### 2.9.3. Erosion distribution mapping

Using ArcGIS, the Kriging method was applied as a geostatistical interpolation technique to predict values at unsampled locations based on spatial autocorrelation among observed points. The method estimates the value at location  $x_0$  as a weighted linear combination of neighbouring observations by Eq. 3:

$$Z(x_0) = \sum_{i=1}^n \lambda_i Z(x_i) \tag{3}$$

where  $Z(x_0)$  is the estimated value at location  $x_0$ ,  $Z(x_i)$  are the observed values at surrounding locations,  $\lambda i$  are the kriging weights assigned to each observation, and n is the number of data points used in the interpolation. The weights were derived by minimising the estimation variance in Eq. 4:

$$\sigma_{k}^{2}(x_{0}) = Var[Z(x_{0}) - Z(x_{0})] \tag{4}$$

Using the semi-variance function  $\gamma(x_i,x_0)$  obtained from the variogram model. This optimisation yielded the best linear unbiased estimator for spatial prediction. Uncertainty estimates from the kriging variance were generated across the interpolation grid, and the resulting uncertainty maps are provided in the supplementary data.

#### 2.9.4. Distribution of soil nutrients across soil particle size fractions

Quantification of soil nutrient distribution across various soil particle size fractions (SPSF) is shown in Eq. 5:

$$MNi = \sum_{i=1}^{6} (SPSF(MNs)i * SPSF(proportion)i)$$
 (5)

Where MNi is the concentration of micronutrients in bulk agricultural soils, SPSF(MNs)i is nutrient concentrations in specific soil particle size, and SPSF (proportion)i is the percentage of soil particle fraction from the entire bulk soil.

#### 2.9.5. Quantification of soil nutrient loss/gain across SPF

The extent of soil nutrient loss or gain across particle sizes in relation to soil erosion or deposition is described in Eq. 6:

$$\textit{MNs}_r = \left(\frac{\textit{SPSF proportion}}{100}\right) \times (\textit{erosion or deposition}) \times (\textit{SPSF mns})$$
 (6)

Where  $MNs_r$  is the quantity of micronutrients lost or gained after soil movement measured in (t ha<sup>-1</sup> yr<sup>-1</sup>), *SPSF proportion* is the proportion amount of soil particle sizes, *erosion/deposition* is the quantities of soil lost or gained per year (t ha<sup>-1</sup> yr<sup>-1</sup>) and *SPSF mns* is the quantity of micronutrients per specific particle size fraction of soil (mg kg<sup>-1</sup>).

#### 3. Results and discussion

#### 3.1. Temporal soil erosion/deposition changes

Fig. 3 illustrates the spatial distribution and temporal changes in soil erosion across three experimental plots in the Oroba Valley, western Kenya, between 2021 and 2023. The interpolated maps reveal distinct variations in erosion and deposition rates (t ha-1 yr-1), highlighting significant soil loss and accumulation areas. Fig. 4 presents the uncertainty analysis derived from Ordinary Kriging, providing insights into the reliability of the spatial patterns of soil redistribution inferred from the <sup>239+240</sup>Pu tracer data. In 2021, Plot 1 and 3 experienced an overall net deposition, with 0.30 t ha<sup>-1</sup> yr<sup>-1</sup> and 0.72 t ha<sup>-1</sup> yr<sup>-1</sup>, respectively. In contrast, Plot 2 showed an overall soil loss of 1.66 t ha<sup>-1</sup> yr<sup>-1</sup> net since 1963. By 2023, Plot 1 and 2 showed net loss soil redistribution of 0.58 t ha<sup>-1</sup> yr<sup>-1</sup> and 0.51 t ha<sup>-1</sup> yr<sup>-1</sup>, respectively. In Plot 3, after encroachment by farmers in 2023, soil loss has been 0.43 t ha<sup>-1</sup> yr<sup>-1</sup>. Fig. 3 also shows cumulative soil erosion across the three plots between the two sampling periods (2021–2023) at rates of  $13.68 \pm 3.9 \text{ t ha}^{-1}$ yr  $^{-1}$  , 6.09  $\pm$  3.2 t  $ha^{-1}$  yr  $^{-1}$  , and 0.32  $\pm$  3.6 t  $ha^{-1}$  yr  $^{-1}$  for Plots 1, 2, and 3, respectively.

These results highlight the impact of human activity on erosion-prone encroachment, thus accelerating degradation. Conversion of natural landscapes to arable land coupled with conventional tillage systems, reduced vegetative cover, destabilised soil aggregates, and altered hydrology, increasing runoff and sediment transport (García-Ruiz et al., 2013; Lal, 2019; Borrelli et al., 2020). Average erosion rate from the study plots surpassed the globally recognised tolerable soil loss thresholds of 1–10 t ha<sup>-1</sup> yr<sup>-1</sup> (Verheijen et al., 2009; Panagos et al., 2014; Fenta et al., 2020), highlighting the severity of geomorphic instability in the study area. The values recorded, particularly in Plot 1 (13.68  $\pm$  3.9 t ha<sup>-1</sup> yr<sup>-1</sup>), align with findings by Montgomery (2007), Nearing et al. (2017), and Pimentel and Burgess (2013) who posited that such high rates of soil loss pose significant threats to long-term agricultural sustainability and food security.

In Plot 2, terrace drop heights ranging from 1.5 m to 3.5 m appear ineffective due to structural deficiencies and poor maintenance. Degraded terraces worsen erosion by limiting infiltration, increasing runoff, and reducing sediment retention (Poesen et al., 2003; Morgan, 2009; García-Ruiz et al., 2013). Tillage erosion causes substantial soil redistribution in sloping landscapes. It is an important driver of in-field biomass patterns in intensively cultivated hummocky terrain (Ottl et al., 2021, 2022). In Sections 1 and 2 of the plots, tillage erosion may have contributed significantly to the observed soil loss. To establish terraces, the farmer has progressively moved soil downslope using an ox-drawn plough. Poor maintenance intensifies soil loss (Bakker et al., 2005; Boardman et al., 2022), consistent with high erosion rates in Plot 2 terraces (19-26 t ha<sup>-1</sup> yr<sup>-1</sup>) (Fig. 3). Farmer encroachment and tillage on Plot 3 have altered surface cover and soil structure, increasing erosion vulnerability. This disturbance shifted the sediment budget from net deposition to net erosion, as shown in soil redistribution data (Fig. 3). Tillage shifts soil, disrupts soil aggregation, breaks down macro-aggregates, and exposes the surface to raindrop impact, accelerating detachment and transport. (Blanco-Canqui and Lal, 2008; Korba et al., 2024; Juřicová et al., 2025).

#### 3.2. The impact of erosion on particle size distribution over time

Soil particle size fractions (SPSFs)  $<10~\mu m$ ,  $10~\mu m$   $-25~\mu m$ , and  $25~\mu m$   $-50~\mu m$  generally decreased downslope (S1 - highest elevation—S5/S6 - lowest elevation) in 2021 and 2023, while course fractions (100  $\mu m$   $-500~\mu m$  and 500  $\mu m$   $-2000~\mu m$ ) increased downslope across all plots (Fig. 5). On average, Plot 1 exhibited a reduction of -3.3~% in the  $<10~\mu m$  SPSF, accompanied by a notable increase of 6.4 % in the 500 $\mu m$ -2000 $\mu m$  fraction. Similarly, Plot 2 showed an increase of 3.0 % in the  $500\mu m$ -2000 $\mu m$  fraction. Although other particle size fractions

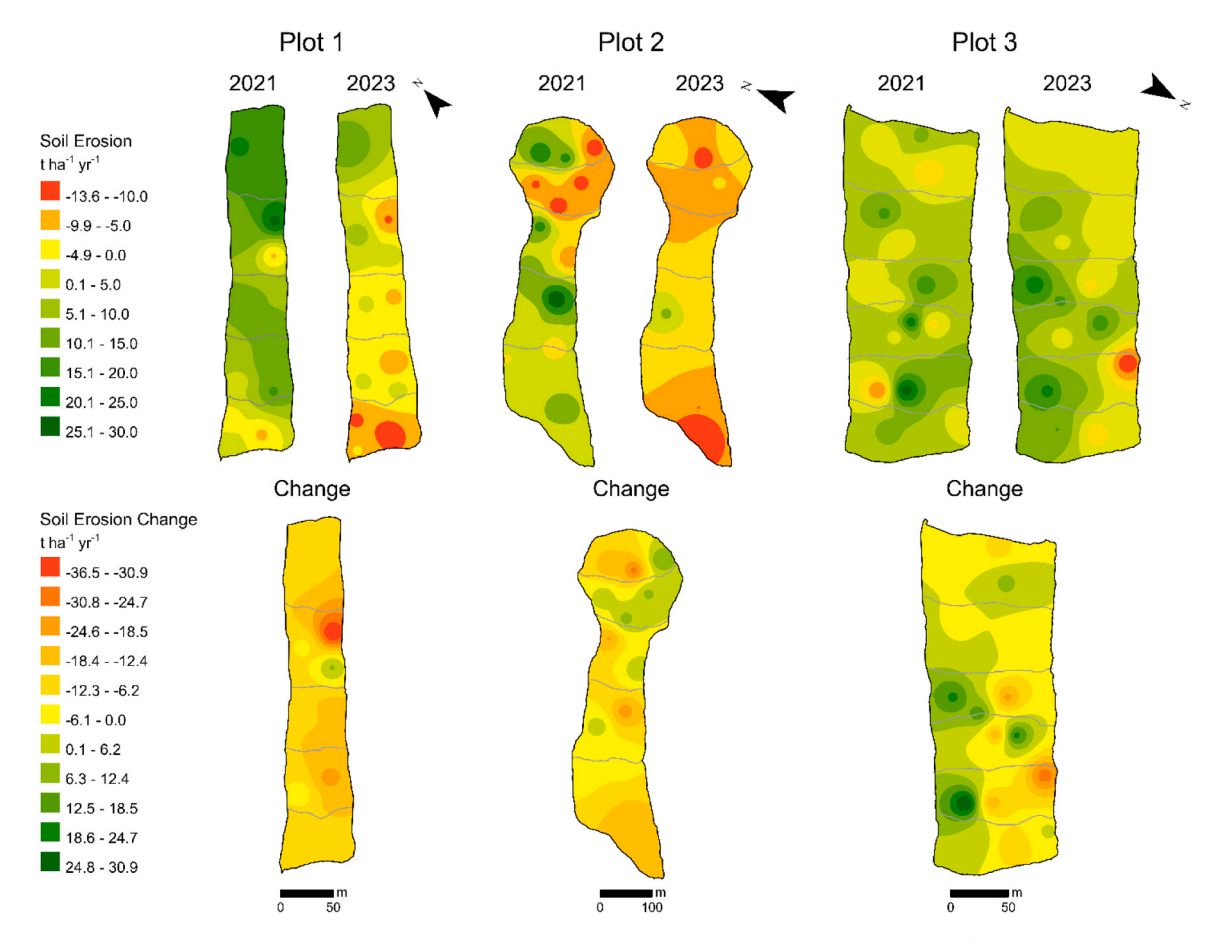


**Fig. 3.** Spatial patterns of soil erosion and erosion change in three experimental plots in the Oroba Valley, western Kenya, between 2021 and 2023. The top panels show interpolated soil erosion rates (t ha<sup>-1</sup> yr<sup>-1</sup>) for each plot in 2021 and 2023. The bottom panels illustrate the net change in soil erosion between the two years, with positive values indicating deposition (green) and negative values indicating net soil loss (red).

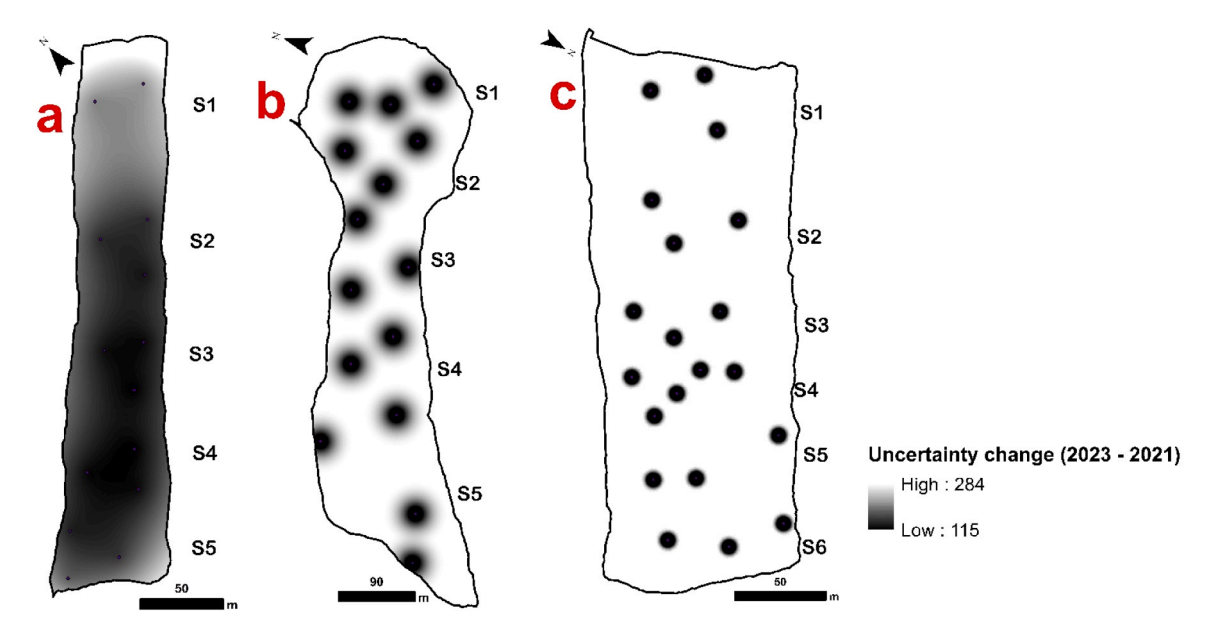


Fig. 4. Uncertainty from Ordinary Kriging from the Spatial patterns of soil erosion change in three experimental plots in the Oroba Valley, western Kenya, between 2021 and 2023.

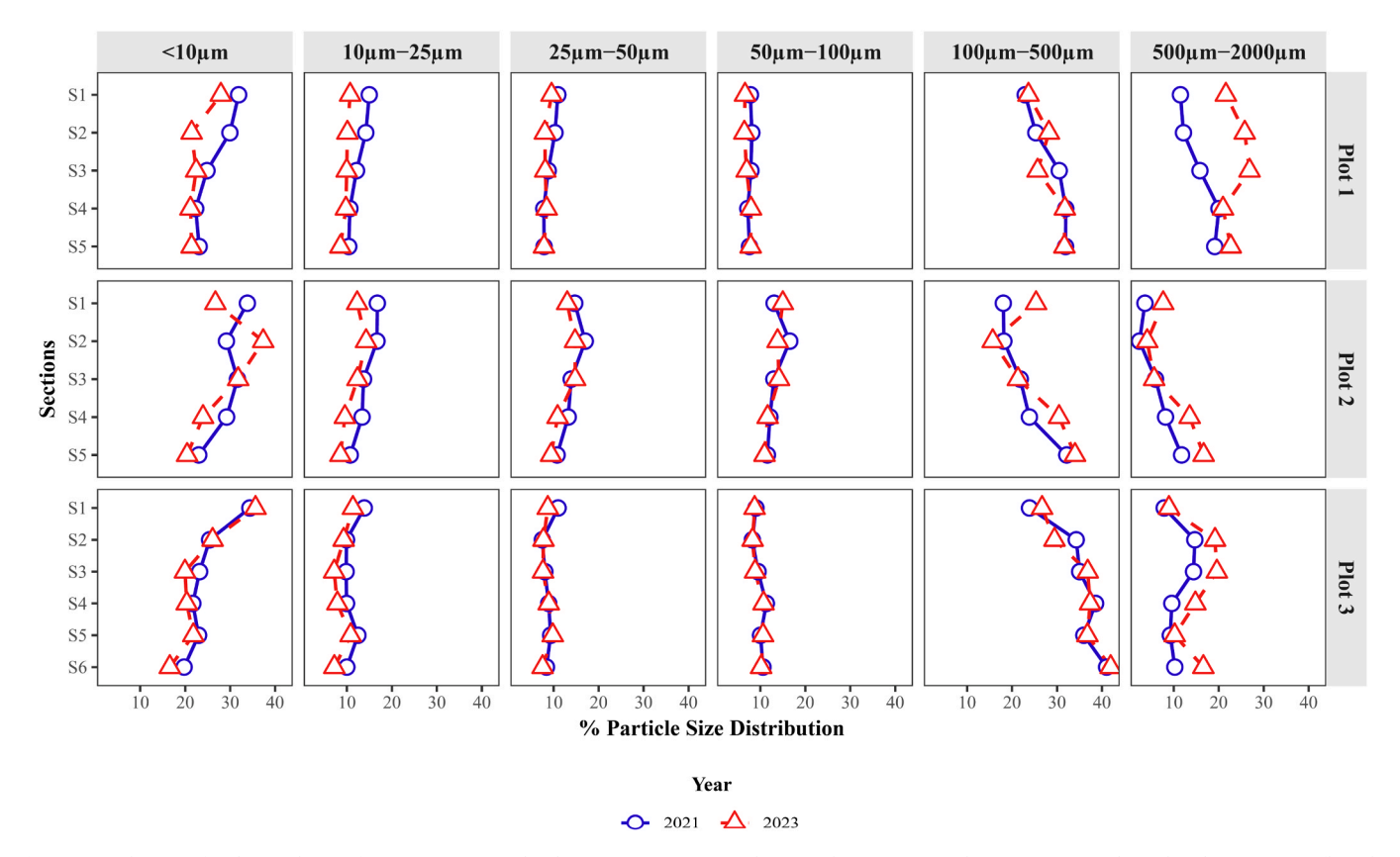


Fig. 5. Distribution of soil particle size fractions across study plot sections in 2021 and 2023. The percentage changes in SPSFs along the plot sections reflect the influence of land management practices on soil texture dynamics over time.

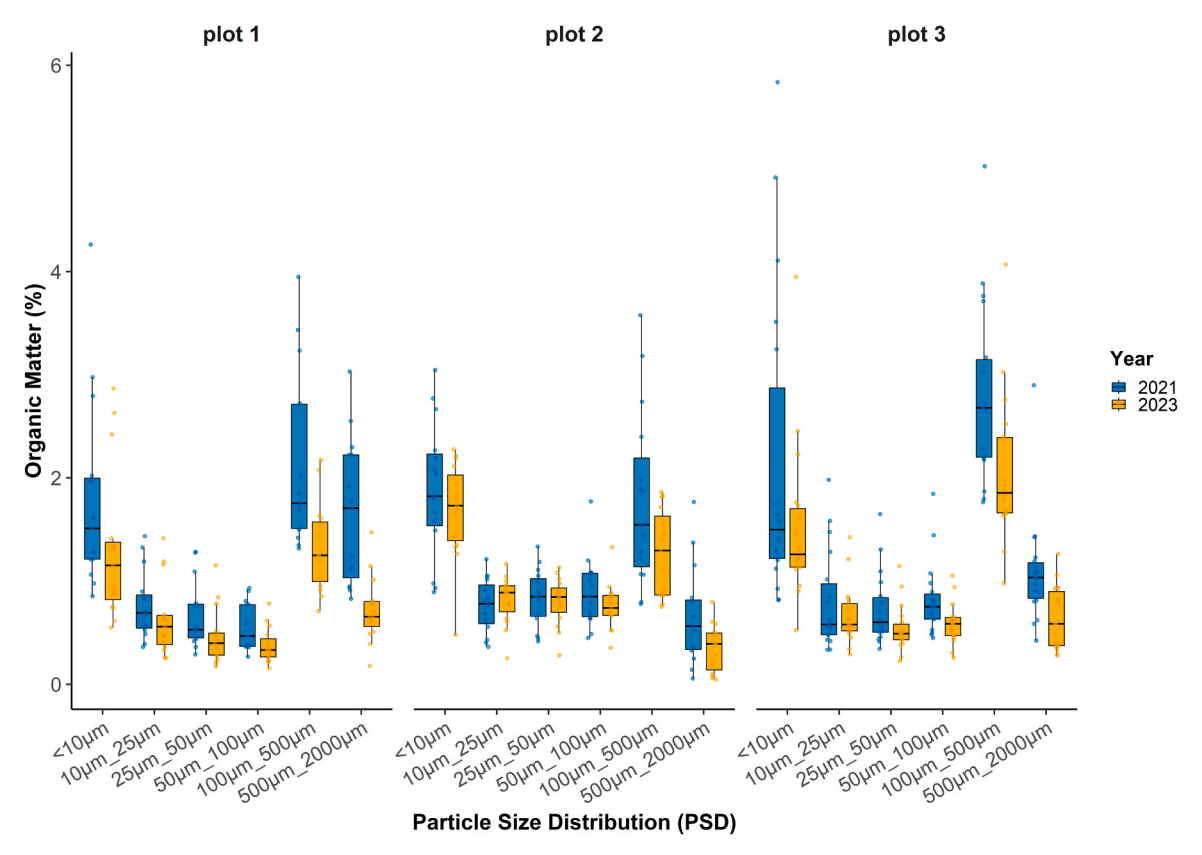


Fig. 6. Distribution of eroded percentage organic matter (OM, %) across particle size fractions in three study plots (Plot 1-3) for the years 2021 and 2023.

demonstrated variations along the slope between sampling years, these changes were not statistically significant (p-value >0.05).

# 3.3. Temporal and spatial dynamics of organic matter across soil particle size fractions

Fig. 6 shows the distribution of eroded OM across particle size fractions in three study plots for the years 2021 and 2023. The OM content were consistently higher in the fine fractions (<10 µm and  $10-25 \mu m$ ) compared to coarser fractions (>100  $\mu m$ ), highlighting the strong role of fine particles in OM retention through mineral surface protection and organo-mineral interactions. A temporal decline in OM was evident between 2021 and 2023 across most particle size classes, with the reductions particularly marked in the fine and intermediate fractions. Between 2021 and 2023, significant reductions in OM were observed in several SPSFs within Plots 1 and 2. In Plot 1, a notable decrease of OM was recorded in the 500  $\mu m$  –2000  $\mu m$  fraction, where it decreased from 0.908 % in 2021–0.187 % in 2023 (p-value < 0.05). Plot 2 exhibited the most pronounced and widespread losses in OM across nearly all SPSFs. Specifically, significant reductions (p-value <0.05) were found in the  $< 10 \mu m$  (Percentage decrease: 0.96 %),  $10 \mu m$ –25  $\mu m$ (0.48 %), 25  $\mu$ m $-50 \mu$ m (0.43 %), 50  $\mu$ m $-100 \mu$ m (0.36 %), and 100 μm–500 μm (0.12 %) fractions, indicating the high rate of OM depletion across both fine and intermediate soil fractions in this plot. Conversely, in Plot 3, although slight decreases in OM were observed across all SPSFs, none of the changes were significant (p-value > 0.05), suggesting comparatively stable OM levels over the study period.

The temporal loss of OM observed in Plots 1 and 2 may be attributed to the effects of conventional cultivation practices, which disrupt soil aggregates and diminish vegetation cover, thereby intensifying soil erosion and facilitating the removal of OM and associated nutrients (Johnston et al., 2017; Agric4Profits, 2023). This phenomenon is illustrated in Fig. 6, where a pronounced erosion of  $< 100 \, \mu m$  particles in Plots 1 and 2 corresponds with significant OM losses. These findings further suggest that tillage-induced soil disturbance disproportionately compromises the soil's capacity to retain OM, particularly in eroded soils (Öttl et al., 2021). Tillage-induced soil disturbance breaks down stable soil aggregates, which are critical for protecting OM from microbial decomposition and physical removal. When aggregates are disrupted, previously protected OM becomes exposed to oxidation and is more easily mobilized by erosive forces such as wind and water (Six et al., 2000; Denef et al., 2001; Lal, 2003; Weidhuner et al., 2021). In eroded soils, this effect is even more pronounced because the loss of fine particles (<100 µm), which have a high surface area and strong capacity to adsorb and stabilize OM, further reduces the soil's ability to retain organic carbon and nutrients (VandenBygaart et al., 2012; Wiesmeier et al., 2019). Consequently, repeated tillage accelerates the decline of soil organic matter stocks and weakens soil resilience against degradation.

Despite more visible OM loss in < 100 µm particles, the statistical strength was more pronounced in macroaggregates, indicating potential OM redistribution or preferential association with 100  $\mu m$  -2000  $\mu m$ particles due to the high intensity of cultivation, as indicated by the farmer from Plot 2. Although the farmer reported that they are currently practising non-inversion tillage, the amount of OM lost was relatively high, consistent with Ottl et al. (2022), which demonstrates that non-inversion chisel tillage can result in significantly greater soil translocation than inversion mouldboard tillage, particularly under dry, sandy conditions, challenging the common perception of non-inversion tillage as a soil-conserving practice. Plot 2 showed a significant loss of OM across all SPSFs (p-value < 0.05), with the  $<10\,\mu m$  fraction exhibiting more loss at 0.96 % (Fig. 5). Fine SPSFs ( $<10 \mu m$ ) have high surface areas that promote OM adsorption. Their low settling velocities allow them to remain suspended in overland flow, increasing susceptibility to erosion and leading to disproportionate OM loss from the soil matrix (Lin et al., 2022; Hofbauer et al., 2023; Wang et al., 2024). Plot 3

exhibited the lowest OM loss across all SPSFs, with a reduction of 0.28 %. This implies that land cover and the absence of tillage are critical in minimising nutrient and OM losses. (Blanco-Canqui and Lal, 2008; Korba et al., 2024). Land cover protects the soil surface from raindrop impact and erosion, while plant roots enhance aggregate stability, infiltration, and nutrient uptake. The absence of tillage maintains soil structure, reduces oxygen exposure of protected organic matter, and slows microbial decomposition, thereby conserving soil organic carbon. Together, these processes minimise both particulate and dissolved nutrient losses, improving soil fertility and reducing off-site pollution (Tan et al., 2015; Daryanto et al., 2017; Farmaha et al., 2022).

## 3.4. Temporal changes of soil nutrients eroded across soil particle size fractions

Fig. 7 shows the distribution of essential plant and animal nutrients across soil particle size fractions (SPSFs) in three study plots for the years 2021 and 2023. Concentrations of micronutrients (Cu, I, Se, Mn, Mo, Zn) and macronutrients (Fe, Mg, Na, Ca, K, P) exhibit distinct patterns along the SPSFs continuum, with finer fractions ( $<100~\mu m$ ) generally retaining higher nutrient concentrations compared to coarser fractions ( $>100~\mu m$ ). Temporal comparisons between 2021 and 2023 reveal a decline in nutrient retention in some size fractions, particularly in the fine particles, indicating that soil erosion and cultivation practices may drive nutrient depletion. The variation across plots further highlights the influence of site-specific management and erosion dynamics on nutrient partitioning within soil aggregates.

In Plot 1 during 2021, all nutrients were reduced with increased particle size up to 100 µm. A significant (p-value <0.05) increase in nutrient concentration was observed for the subsequent SPSFs  $(100-2000 \mu m)$ . This trend was the opposite during 2023. For Plot 2, nutrient concentrations remained at an average constant during 2021 in all SPSFs, while they reduced variably in 2023. Both macro- and micronutrient concentrations in Plot 3 had a similar trend between the two sampling periods (2021 & 2023) of a slight decrease within the finer soil particles (<100 μm), while an abrupt increase occurred within 100 μm  $-500 \mu m$ , followed by a decrease in the coarse SPSFs (500–2000  $\mu m$ ). Between the two years (2021-2023), iodine showed a significant decrease (p-value <0.05) across all SPSFs in plot 1. Selenium in Plot 1 was significantly lost in  $>100\ \mu m$  SPSFs, generally with an average of 0.05 mg kg $^{-1}$  (p-value <0.05), while in Plot 2, more was lost in 10  $\mu$ m  $^{-1}$  $50 \, \mu m$  with an average of  $0.04 \, mg \, kg^{-1}$  lost in the study years. Significant (p-value < 0.05) P loss between 2021 and 2023 was observed in Plot 1 across all SPSFs and in Plot 2 within the 10 µm-100 µm range. In contrast, Plot 3 showed no significant difference (p-value >0.05) in 10  $\mu m$  to 100  $\mu m$  as seen in Fig. 5. In Plot 1, the 500 $\mu m$ -2000 $\mu m$  fraction showed a decrease in Na, dropping from 2166 mg kg<sup>-1</sup> to 502 mg kg<sup>-1</sup> with a p-value < 0.05. In Plot 2, degradation occurred in the 10μm-25 μm and 25 μm-50 μm size fractions, where Na concentrations decreased by 1257 mg  $\mathrm{kg}^{-1}$  and by 1139 mg  $\mathrm{kg}^{-1}$ , respectively. Magnesium showed significant reductions in Plot 1 at 500 µm - 2000 µm of  $256~mg~kg^{-1}~(p\text{-values}~<~0.05)$  and Plot 2 at  $10~\mu m$  -  $25~\mu m$  of 1127 mg kg $^{-1}$  (p-values < 0.05), respectively. Significant loss of K was most pronounced in 500  $\mu m$  - 2000  $\mu m$  and 100  $\mu m$  -500  $\mu m$  by 1457  $mg~kg^{-1}$  and 1136  $mg~kg^{-1}$  (p-values < 0.05), respectively, only in Plot 1. Similarly, Ca is also lost in 500  $\mu m$  - 2000  $\mu m$  and 100  $\mu m$  $-500 \, \mu \text{m}$  by  $1786 \, \text{mg kg}^{-1}$  and  $1980 \, \text{kg}^{-1}$  (p-values < 0.05), respectively.

In Plot 2, Cu significantly (p-values <0.05) declines by 2.33 mg kg $^{-1}$  in the 10  $\mu m$  - 25  $\mu m$  fraction. Manganese, Fe, and Zn showed consistent negative trends in Plots 1 and 2 across all SPSFs, with no significant difference (p-value  $>\!0.05$ ). In contrast, Plot 3 remained stable across all elements (p-values  $>\!0.05$ ), except for slight, non-significant increases in Mn, Fe, and Mo (Fig. 6). These results are consistent with Li et al. (2023) and Zhang et al. (2024) Who report that erosion-driven sediment sorting and the selective transport of fine, nutrient-rich particles, particularly

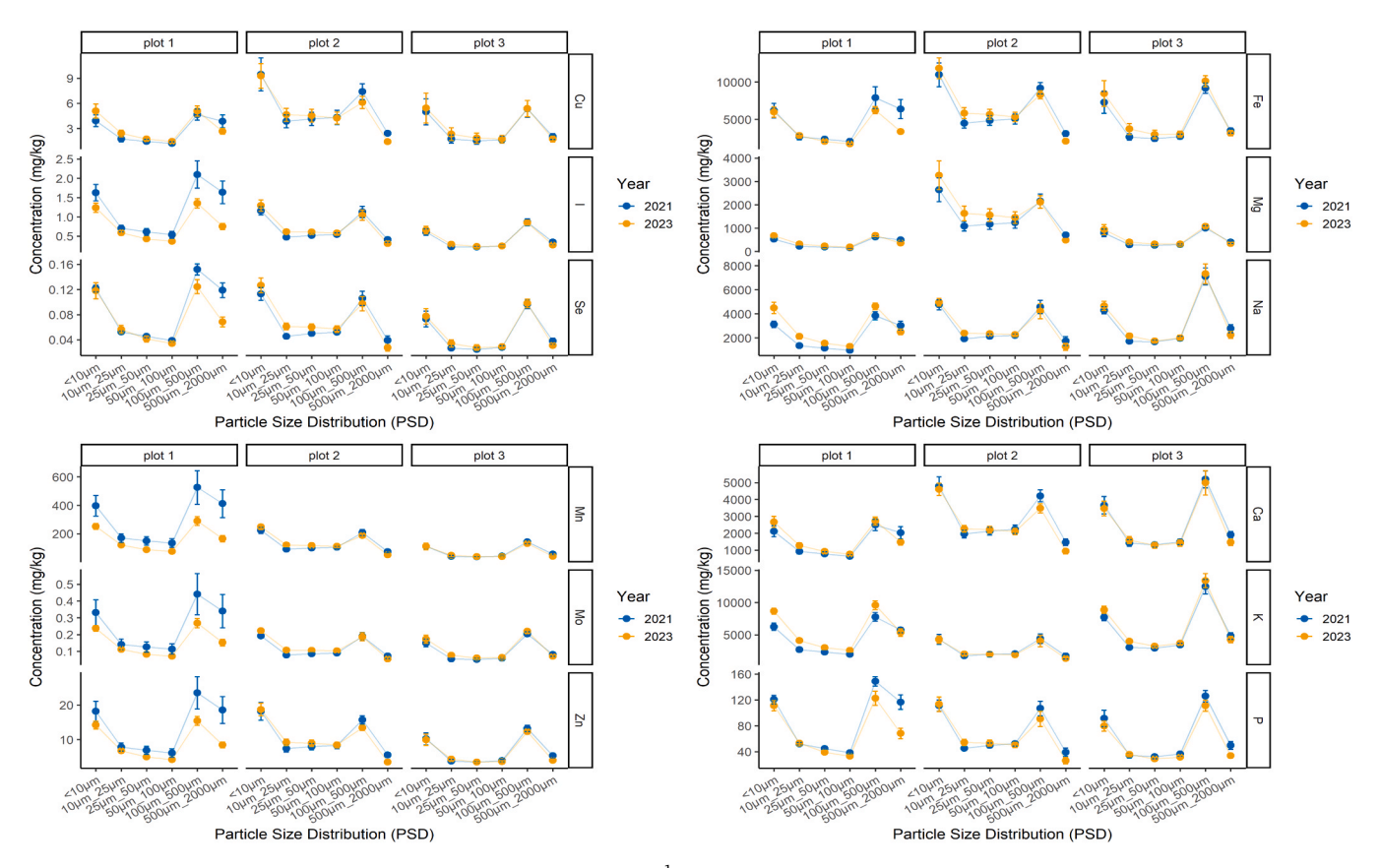


Fig. 7. Changes in soil nutrient concentration (mg kg<sup>-1</sup>) for different soil particle size fractions from 2021 to 2023.

those bound to fine particle fractions, are key drivers of vertical and lateral nutrient redistribution, with smaller particles being more susceptible to erosion due to overland flow and lower settling velocities in water. The significant decline of Cu in the  $10-25~\mu m$  fraction reflects the preferential loss of fine particles with high surface reactivity and strong metal-binding capacity. The fact that fine particles possess high surface area, abundant reactive sites, and strong affinities for OM and metal oxides, making them primary carriers of Cu; once mobilised by erosion, their selective removal leads to disproportionate Cu depletion in the soil matrix (Alloway, 1995, 2012; Caporale and Violante, 2016).

Unlike Plots 1 and 2, which exhibited significant nutrient degradation (p-value < 0.05) due to erosion in different SPSFs, Plot 3 showed no significant variation, indicating enhanced nutrient stability likely attributable to shrub cover mitigating erosion. These observations are consistent with findings by Bashagaluke et al. (2018), who reported increased seasonal nutrient depletion associated with overcropping and monocropping by the tilling system of farming. Nutrient loss analysis showed element-specific trends tied to particle size affinity, varying with land management and topography, consistent with findings by Zhang et al. (2011) on nutrient redistribution influenced by particle association and landscape features. Plot 1 showed substantial nutrient loss between 2021 and 2023, mainly linked to larger soil particles (100  $\mu$ m-2000  $\mu$ m), especially along the lower part of the slope. Nutrients such as K, Na, Ca, and Mg, commonly hosted in primary minerals (e.g., feldspars, micas, calcite) within 100 µm-500 µm particles, are mobilised during erosion as coarse particles detach and move with runoff, transporting nutrients in the solid phase rather than dissolved form (Murrell et al., 2021). Iodine, P, Ca, Mn, Zn, Mo, Co, and Se were mainly lost in the 100  $\mu m$  $-500 \, \mu m$  fraction, with minimal loss in the  $50 \, \mu m$   $-100 \, \mu m$  range (p-value < 0.05). Both Mg and Fe remained evenly distributed across particle sizes, with minimal losses along the elevation. Losses of micronutrients (Se, Mo, Cu) and macronutrients (P, Ca) indicate a strong geochemical tendency to bind with mineral-associated particles. Hunt

and Sahimi (2024) demonstrated that these elements commonly associate with calcium phosphates or Mn/Fe oxides in medium-sized SPSF, and the slight decline in the 50–100  $\mu$ m range in Plot 1 suggests their reduced mobility under prevailing erosion dynamics. The stable distribution of Mg and Fe suggests strong binding within resistant minerals or organic complexes, limiting loss through runoff (Zheng et al., 2016). In support, Goulding et al. (2021) show that K and Na can be lost in large particle fractions when the soil is significantly disturbed.

The nutrient distribution in Plot 2 was notably affected in the upper part of the slope (S1 and S2), where certain elements were slightly accumulated. However, significant nutrient loss was recorded in sections S1, S3, and S4. Unlike Plot 1, nutrient loss in Plot 2 was more pronounced in the finer soil particle fraction (<50  $\mu$ m), such as iodine, P, Ca, Mn, Zn, Mo, Cu, and Se, with the highest loss occurring in section S4. These reinforce the traditional erosion model that indicates clay and silt particles are more easily transported downhill due to their lightweight and colloidal properties (Zhao et al., 2022). Interestingly, the increase in Mg and Fe in S4, despite the initial loss in S1, implies potential deposition and aggregation occurring downstream, a trend that is modelled using sediment tracing at the field scale (Hall et al., 2015; Chadwick and Asner, 2016; Bukombe et al., 2022).

Plot 3, which remained largely unfarmed and had been encroached on within two years, showed signs of nutrient loss across all SPSFs, although the difference was insignificant (p-value  $>\!0.05$ ). The indication of loss of nutrients across all particle size fractions suggests that soil disturbance due to encroachment through vegetation clearing and tillage has significantly impacted soil structure (Elnaggar, 2020; Sanogo et al., 2023; Du et al., 2024). The substantial nutrient loss observed in section S6 likely reflects the effects of concentrated surface runoff or recent vegetation removal, which left the soil exposed and vulnerable to erosion (Zhao et al., 2023, 2024). Interestingly, the localised increase in K within the 100  $\mu m$  –500  $\mu m$  fraction in S3 may point to anthropogenic influences, such as the application of ash, compost, or localised

fertilisation (Bungau et al., 2021; Tian et al., 2022; Qu and Han, 2023). Alternatively, it could result from the redistribution of nutrients from upslope areas. Potassium in weathered tropical soils often accumulates in coarser primary minerals such as feldspars, which are typically retained in the  $100 \ \mu m$  – $500 \ \mu m$  particle size range (Yan et al., 2022).

#### 4. Conclusion

This study effectively demonstrated the precision of using  $^{239+240}\text{Pu}$ isotopes to trace and quantify soil redistribution across agroecosystems, irrespective of land management practices. Three agricultural landscapes in the Nandi Hills of Kenya were investigated to assess the erosion-deposition dynamics and their influence on the spatial and temporal gains and losses of nutrients across different soil particle size fractions. When integrated with particle size distribution and nutrient profiling, the MODERN model successfully quantifies both soil redistribution and the associated macro- and micronutrient fluxes. This enabled detailed spatial and temporal mapping and determination of nutrient loss, particularly within the most erosion-prone fine particle fractions. Soil erosion exhibited significant variation depending on land management practices and the duration of cultivation. Long-time established plots (Plots 1 and 2) experienced overall net soil losses (up to 13.68 t ha<sup>-1</sup> yr<sup>-1</sup>), surpassing globally recognised tolerable limits of 10 t ha<sup>-1</sup> yr<sup>-1</sup>. In contrast, recently cultivated or undisturbed plots (Plot 3) initially exhibited net deposition, which transitioned to net erosion following land disturbance. Erosion predominantly affected fine soil particles (<100 µm), rich in OM and essential nutrients such as Se, Zn, P, and I. The fine fractions were highly susceptible to overland flow, indicating that erosion reduces soil quantity and significantly diminishes quality and fertility. In Plot 2, tillage erosion, in addition to poor maintenance and lack of knowledge of the procedural quality of terrace construction, resulted in high recorded erosion rates. Therefore, effective soil erosion mitigation strategies should be implemented before cultivation, especially in steep terrains, focusing on preserving fine soil particles and organic matter content.

#### CRediT authorship contribution statement

Odipo Osano: Writing – review & editing, Resources, Funding acquisition, Conceptualization. Michael J. Watts: Writing – review & editing, Supervision, Project administration, Funding acquisition, Conceptualization. Humphrey Olivier S: Writing – review & editing, Supervision, Methodology, Funding acquisition, Conceptualization. Ruth Njoroge: Writing – review & editing, Validation, Supervision. Job Isaboke: Writing – original draft, Methodology, Investigation, Formal analysis, Data curation, Conceptualization.

#### **Funding**

This research was supported by The Royal Society (ICA\R1 \1910770), the NERC-UKRI ODA- National Capability Foundation Award (NE/R000069/1), the NERC National Capability Science International Award (NE/X006255/1), and the British Geological Survey University Funding Initiative (STU/2023/011). This work is published with the permission of the Executive Director of the British Geological Survey.

#### **Declaration of Competing Interest**

The authors declare no known financial or personal conflicts of interest that could have influenced the findings or interpretations presented in this study.

#### Acknowledgments

We appreciate all those who assisted in collecting samples, including

the field and laboratory staff at the biotechnology lab at the University of Eldoret, and the Inorganic Geochemistry Facility. We also thank Sophia Dowell and David King for their valuable knowledge in the laboratory.

#### Appendix A. Supporting information

Supplementary data associated with this article can be found in the online version at doi:10.1016/j.still.2025.106962.

#### Data availability

Data will be made available on request.

#### References

- Agric4Profits. (2023). Soil degradation due to continuous cropping. Retrieved April 9 from (https://agric4profits.com/soil-degradation-due-to-continuous-cropping/).
- Ahmed, M., Hasanuzzaman, M., Raza, M.A., Malik, A., Ahmad, S., 2020. Plant nutrients for crop growth, development and stress tolerance. In: Roychowdhury, R., Choudhury, S., Hasanuzzaman, M., Srivastava, S. (Eds.), Sustainable Agriculture in the Era of Climate Change. Springer, pp. 43–92. https://doi.org/10.1007/978-3-030.45569.63
- Alewell, C., Pitois, A., Meusburger, K., Ketterer, M., Mabit, L., 2017. 239+240pu from "contaminant" to soil erosion tracer: Where do we stand? Earth Sci. Rev. 172, 107–123. https://doi.org/10.1016/j.earscirev.2017.07.009.
- Alloway, B., 1995. Soil processes and the behaviour of metals. Heavy Met. Soils 13, 3488.Alloway, B.J., 2012. Heavy metals in soils: Trace metals and metalloids in soils and their bioavailability, 22. Springer Science & Business Media.
- Arata, L., Alewell, C., Frenkel, E., A'Campo-Neuen, A., Iurian, A.-R., Ketterer, M.E., Mabit, L., Meusburger, K., 2016. Modelling deposition and erosion rates with radionuclides (modern) part 2: a comparison of different models to convert 239+240pu inventories into soil redistribution rates at unploughed sites. J. Environ. Radioact. 162-163, 97–106. https://doi.org/10.1016/j.jenvrad.2016.05.009.
- Arata, L., Meusburger, K., Frenkel, E., A'Campo-Neuen, A., Iurian, A.-R., Ketterer, M.E., Mabit, L., Alewell, C., 2016. Modelling deposition and erosion rates with radionuclides (modern) part 1: A new conversion model to derive soil redistribution rates from inventories of fallout radionuclides. J. Environ. Radioact. 162-163, 45–55. https://doi.org/10.1016/j.jenvrad.2016.05.008.
- Bakker, M.M., Govers, G., Kosmas, C., Vanacker, V., Oost, K. v, Rounsevell, M., 2005. Soil erosion as a driver of land-use change. Agric. Ecosyst. Environ. 105 (3), 467–481. https://doi.org/10.1016/j.agee.2004.07.009.
- Bashagaluke, J.B., Logah, V., Opoku, A., Sarkodie-Addo, J., Quansah, C., 2018. Soil nutrient loss through erosion: Impact of different cropping systems and soil amendments in ghana. PLoS One 13 (12), e0208250. https://doi.org/10.1371/ journal.pone.0208250.
- Bizmark, N., Schneider, J., Priestley, R.D., Datta, S.S., 2020. Multiscale dynamics of colloidal deposition and erosion in porous media. Sci. Adv. 6 (46), eabc2530. https://doi.org/10.1126/sciadv.abc2530.
- Blanco-Canqui, H., Lal, R., 2008. No-tillage and soil-profile carbon sequestration: An on-farm assessment. Soil Sci. Soc. Am. J. 72 (3), 693–701.
- Boardman, J., Poesen, J., Evans, M., 2022. Slopes: soil erosion. In: Burt, T.P., Goudie, A. S., Viles, H.A. (Eds.), The History of the Study of Landforms Or the Development of Geomorphology: Volume 5: Geomorphology in the Second Half of the Twentieth Century. Geological Society of London. https://doi.org/10.1144/m58-2021-4.
- Borrelli, P., Robinson, D.A., Panagos, P., Lugato, E., Yang, J.E., Alewell, C., Wuepper, D., Montanarella, L., Ballabio, C., 2020. Land use and climate change impacts on global soil erosion by water (2015-2070). Proc. Natl. Acad. Sci. 117 (36), 21994–22001. https://doi.org/10.1073/pnas.2001403117.
- Bukombe, B., Bauters, M., Boeckx, P., Cizungu, L.N., Cooper, M., Fiener, P., Kidinda, L.K., Makelele, I., Muhindo, D.I., Rewald, B., Verheyen, K., Doetterl, S., 2022. Soil geochemistry and not topography as a major driver of carbon allocation, stocks, and dynamics in forests and soils of african tropical montane ecosystems. N. Phytol. 236 (5), 1676–1690. https://doi.org/10.1111/nph.18469.
- Bungau, S., Behl, T., Aleya, L., Bourgeade, P., Aloui-Sossé, B., Purza, A.L., Abid, A., Samuel, A.D., 2021. Expatiating the impact of anthropogenic aspects and climatic factors on long-term soil monitoring and management. Environ. Sci. Pollut. Res. 28 (24), 30528–30550. https://doi.org/10.1007/s11356-021-14127-7.
- Caporale, A.G., Violante, A., 2016. Chemical processes affecting the mobility of heavy metals and metalloids in soil environments. Curr. Pollut. Rep. 2 (1), 15–27. https://doi.org/10.1007/s40726-015-0024-y.
- Chadwick, K.D., Asner, G.P., 2016. Tropical soil nutrient distributions determined by biotic and hillslope processes. Biogeochemistry 127 (2), 273–289. https://doi.org/ 10.1007/s10533-015-0179-z.
- Chi, W., Zhao, Y., Kuang, W., He, H., 2019. Impacts of anthropogenic land use/cover changes on soil wind erosion in china. Sci. Total Environ. 668, 204–215. https://doi. org/10.1016/j.scitotenv.2019.03.015.
- Croft, S., Favalli, A., 2021. Review and evaluation of the spontaneous fission half-lives of 238pu, 240pu, and 242pu and the corresponding specific fission rates. Nucl. Data Sheets 175, 269–287. https://doi.org/10.1016/j.nds.2021.06.003.

- Daryanto, S., Wang, L., Jacinthe, P.-A., 2017. Impacts of no-tillage management on nitrate loss from corn, soybean and wheat cultivation: A meta-analysis. Sci. Rep. 7 (1), 12117. https://doi.org/10.1038/s41598-017-12383-7.
- Denef, K., Six, J., Paustian, K., Merckx, R., 2001. Importance of macroaggregate dynamics in controlling soil carbon stabilization: Short-term effects of physical disturbance induced by dry-wet cycles. Soil Biol. Biochem. 33 (15), 2145–2153. https://doi.org/10.1016/S0038-0717(01)00153-5.
- Dowell, Sophia, Barlow, T.S., Chenery, S.R., Humphrey, O.S., Isaboke, J., Blake, W.H., Osano, O., Watts, M.J., 2023. Optimisation of plutonium separations using teva cartridges and icp-ms/ms analysis for applicability to large-scale studies in tropical soils. Anal. Methods 15 (34), 4226–4235. https://doi.org/10.1039/d3ay01030a.
- Dowell, S.M., Humphrey, O.S., Blake, W.H., Osano, O., Isaboke, J., Marriott, A.L., Watts, M.J., 2022. Plutonium a Soil Eros. Tracer East Afr.
- Dowell, Sophia, Humphrey, O., Isaboke, J., Barlow, T., Blake, W., Osano, O., Watts, M., 2024. Plutonium isotopes can be used to model soil erosion in kenya. Environ. Geochem. Health 46 (9), 338. https://doi.org/10.1007/s10653-024-02084-2.
- Du, Z., Zheng, H., Penuelas, J., Sardans, J., Deng, D., Cai, X., Gao, D., Nie, S., He, Y., Lü, X., Li, M.-H., 2024. Shrub encroachment leads to accumulation of C, N, and P in grassland soils and alters c:N:P stoichiometry: A meta-analysis. Sci. Total Environ. 951, 175534. https://doi.org/10.1016/j.scitotenv.2024.175534.
- Elnaggar, A., 2020. Evaluation of land degradation in agricultural areas within damietta governorate, egypt caused by urban encroachment, salinity, sodicity and loss of fertility. J. Soil Sci. Agric. Eng. 11 (12), 741–749.
- Farmaha, B.S., Sekaran, U., Franzluebbers, A.J., 2022. Cover cropping and conservation tillage improve soil health in the southeastern United States. Agron. J. 114 (1), 296–316. https://doi.org/10.1002/agj2.20865.
- Fenta, A.A., Tsunekawa, A., Haregeweyn, N., Poesen, J., Tsubo, M., Borrelli, P., Panagos, P., Vanmaercke, M., Broeckx, J., Yasuda, H., Kawai, T., Kurosaki, Y., 2020. Land susceptibility to water and wind erosion risks in the east Africa region. Sci. Total Environ. 703, 135016. https://doi.org/10.1016/j.scitotenv.2019.135016.
- García-Ruiz, J.M., Nadal-Romero, E., Lana-Renault, N., Beguería, S., 2013. Erosion in mediterranean landscapes: changes and future challenges. Geomorphology 198, 20–36. https://doi.org/10.1016/j.geomorph.2013.05.023.
- Gomiero, T., 2016. Soil degradation, land scarcity and food security: Reviewing a complex challenge. Sustainability 8 (3), 281. (https://www.mdpi.com/2071-1050/8/3/281)
- Goulding, K., Murrell, T.S., Mikkelsen, R.L., Rosolem, C., Johnston, J., Wang, H., & Alfaro, M.A. (2021). Outputs: Potassium losses from agricultural systems. In T. S. Murrell, R. L. Mikkelsen, G. Sulewski, R. Norton, & M. L. Thompson, Improving potassium recommendations for agricultural crops Cham.
- Hall, S.J., McNicol, G., Natake, T., Silver, W.L., 2015. Large fluxes and rapid turnover of mineral-associated carbon across topographic gradients in a humid tropical forest: Insights from paired 14c analysis. Biogeosciences 12 (8), 2471–2487. https://doi. org/10.5194/be-12-2471-2015.
- Hofbauer, M., Kincl, D., Vopravil, J., Kabelka, D., Vráblík, P., 2023. Preferential erosion of soil organic carbon and fine-grained soil particles—an analysis of 82 rainfall simulations. Agronomy 13 (1), 217. (https://www.mdpi.com/2073-4395/13/1/21
- Huang, B., Yuan, Z., Li, D., Zheng, M., Nie, X., Liao, Y., 2020. Effects of soil particle size on the adsorption, distribution, and migration behaviors of heavy metal(loid)s in soil: A review [10.1039/D0EM00189A]. Environmental Science Processes Impacts 22 (8), 1596–1615. https://doi.org/10.1039/D0EM00189A.
- Humphrey, O.S., Isaboke, J., Osano, O., Aura, C.M., Blake, W.H., Watts, M.J., 2025. Sediment and soil source apportionment using geochemical fingerprinting techniques in the winam gulf, lake victoria. CATENA 255, 109053. https://doi.org/ 10.1016/j.catena.2025.109053.
- Humphrey, Olivier, Osano, O., Aura, C.M., Marriott, A.L., Dowell, S.M., Blake, W.H., Watts, M.J., 2022. Evaluating spatio-temporal soil erosion dynamics in the winam gulf catchment, kenya for enhanced decision making in the land-lake interface. Sci. Total Environ. 815, 151975. https://doi.org/10.1016/j.scitotenv.2021.151975.
- Hunt, A.G., Sahimi, M., 2024. Networks on networks, second ed. IOP Publishing. https://doi.org/10.1088/978-0-7503-5698-5.
- Isaboke, J., Osano, O., Humphrey, O.S., Dowell, S.M., Njoroge, R., Watts, M.J., 2025. Influence of agricultural land use management on soil particle size distribution and nutrient adsorption in western kenya. Chem. Afr. https://doi.org/10.1007/s42250-025-01202-6.
- Jinlong, W., Jinzhou, D., Jian, Z., 2020. Plutonium isotopes research in the marine environment: A synthesis. J. Nucl. Radiochem. Sci. 20, 1–11. https://doi.org/ 10.14494/jnrs.20.1.
- Johnston, A.E., Poulton, P.R., Coleman, K., Macdonald, A.J., White, R.P., 2017. Changes in soil organic matter over 70 years in continuous arable and ley-arable rotations on a sandy loam soil in england. Eur. J. Soil Sci. 68 (3), 305–316. https://doi.org/ 10.1111/ejss.12415.
- Joy, E.J.M., Kumssa, D.B., Broadley, M.R., Watts, M.J., Young, S.D., Chilimba, A.D.C., Ander, E.L., 2015. Dietary mineral supplies in malawi: Spatial and socioeconomic assessment. BMC Nutr. 1 (1), 42. https://doi.org/10.1186/s40795-015-0036-4.
- Juřicová, A., Öttl, L.K., Wilken, F., Chuman, T., Žížala, D., Minařík, R., Fiener, P., 2025.
  Tillage erosion as an underestimated driver of carbon dynamics. Soil Tillage Res.
  245, 106287. https://doi.org/10.1016/j.still.2024.106287.
- Karthika, K.S., Rashmi, I., Parvathi, M.S., 2018. Biological functions, uptake and transport of essential nutrients in relation to plant growth. In: Hasanuzzaman, M., Fujita, M., Oku, H., Nahar, K., Hawrylak-Nowak, B. (Eds.), Plant nutrients and abiotic stress tolerance. Springer, Singapore, pp. 1–49. https://doi.org/10.1007/ 978-981-10-9044-8 1.
- Kathpalia, R., Bhatla, S., 2018. Plant mineral nutrition. In 37–81. https://doi.org/ 10.1007/978-981-13-2023-1\_2.

- Kipkulei, H.K., Bellingrath-Kimura, S.D., Lana, M., Ghazaryan, G., Baatz, R., Matavel, C., Boitt, M., Chisanga, C.B., Rotich, B., Moreira, R.M., Sieber, S., 2024. Agronomic management response in maize (Zea mays l.) production across three agroecological zones of kenya. Agrosystems Geosci. Environ. 7 (1), e20478. https://doi.org/ 10.1002/agg2.20478.
- Korba, J., Brož, P., Hůla, J., Novák, P., Novák, V., 2024. Influence of soil tillage technology on tillage erosion. Res. Agric. Eng. 70 (2).
  Lal, 2003. Soil erosion and the global carbon budget. Environ. Int. 29 (4), 437–450.
- Lal, R., 2019. Accelerated soil erosion as a source of atmospheric co2. Soil Tillage Res. 188, 35–40. https://doi.org/10.1016/j.still.2018.02.001.
- Li, J., Luo, B., Wei, X., Ci, E., Ni, J., Wei, C., Zhong, S., 2023. Transportation of fine particles controlled by particles flocculation is a key feature of soil erosion on gentle slope land. CATENA 232, 107382. https://doi.org/10.1016/j.catena.2023.107382.
- Lin, J., Fang, N., Zhang, Y., Zeng, Y., Yang, D., Dai, W., Wang, L., Shi, Z., 2022. Dynamics of soil organic carbon in different-sized aggregates under splash erosion. J. Soils Sediment. 22 (6), 1713–1723. https://doi.org/10.1007/s11368-022-03189-w.
- Lukashenko, S.N., Edomskaya, M.A., 2022. Plutonium in the environment: Sources, dissemination mechanisms, and concentrations. Biol. Bull. 49 (11), 2081–2107. https://doi.org/10.1134/S1062359022110139.
- Mabit, L., Zapata, F., Dercon, G., Benmansour, M., Bernard, C., & Walling, D. (2014). Guidelines for using fallout radionuclides to assess erosion and effectiveness of soil conservation strategies, [en línea], ed (9201054149).
- Montgomery, D.R., 2007. Soil erosion and agricultural sustainability. Proc. Natl. Acad. Sci. 104 (33), 13268–13272. https://doi.org/10.1073/pnas.0611508104.
- Morgan, R.P.C., 2009. Soil Erosion and Conservation. John Wiley & Sons.
- Murrell, T.S., Mikkelsen, R.L., Sulewski, G., Norton, R., Thompson, M.L., 2021.
  Improving potassium recommendations for agricultural crops. Springer Nature.
- Nearing, M.A., Xie, Y., Liu, B., Ye, Y., 2017. Natural and anthropogenic rates of soil erosion. Int. Soil Water Conserv. Res. 5 (2), 77–84. https://doi.org/10.1016/j. iswr.2017.04.001.
- de Nijs, E.A., Cammeraat, E.L.H., 2020. The stability and fate of soil organic carbon during the transport phase of soil erosion. Earth Sci. Rev. 201, 103067. https://doi. org/10.1016/j.earscirev.2019.103067.
- Öttl, L.K., Wilken, F., Auerswald, K., Sommer, M., Wehrhan, M., Fiener, P., 2021. Tillage erosion as an important driver of in-field biomass patterns in an intensively used hummocky landscape. Land Degrad. Dev. 32 (10), 3077–3091. https://doi.org/ 10.1002/ldr.3968.
- Öttl, L.K., Wilken, F., Hupfer, A., Sommer, M., Fiener, P., 2022. Non-inversion conservation tillage as an underestimated driver of tillage erosion. Sci. Rep. 12 (1), 20704. https://doi.org/10.1038/s41598-022-24749-7.
- Panagos, P., Meusburger, K., Ballabio, C., Borrelli, P., Alewell, C., 2014. Soil erodibility in europe: A high-resolution dataset based on lucas. Sci. Total Environ. 479-480, 189–200. https://doi.org/10.1016/j.scitotenv.2014.02.010.
- Pimentel, D., Burgess, M., 2013. Soil erosion threatens food production. Agriculture 3 (3), 443–463. (https://www.mdpi.com/2077-0472/3/3/443).
- Poesen, J., Nachtergaele, J., Verstraeten, G., Valentin, C., 2003. Gully erosion and environmental change: Importance and research needs. CATENA 50 (2), 91–133. https://doi.org/10.1016/S0341-8162(02)00143-1.
- Qu, R., Han, G., 2023. Potassium isotopes of fertilizers as potential markers of anthropogenic input in ecosystems. Environ. Chem. Lett. 21 (1), 41–45. https://doi. org/10.1007/s10311-022-01516-8.
- Ramteke, P., Ghabane, V., Kadu, P., Kharche, V., Ghosh, S., 2023. Perspective chapter: Conservation and enhancement of soil health for sustainable agriculture. In: Hakeem, K.R. (Ed.), Organic fertilizers new advances and applications. IntechOpen. https://doi.org/10.5772/intechopen.1000869.
- Rashmi, I., Karthika, K.S., Roy, T., Shinoji, K.C., Kumawat, A., Kala, S., Pal, R., 2022. Soil erosion and sediments: A source of contamination and impact on agriculture productivity. In: Naeem, M., Bremont, J.F.J., Ansari, A.A., Gill, S.S. (Eds.), Agrochemicals in Soil and Environment: Impacts and Remediation. Springer Nature, Singapore, pp. 313–345. https://doi.org/10.1007/978-981-16-9310-6\_14.
- Saentho, A., Wisawapipat, W., Lawongsa, P., Aramrak, S., Prakongkep, N., Klysubun, W., Christl, I., 2022. Speciation and ph- and particle size-dependent solubility of phosphorus in tropical sandy soils. Geoderma 408, 115590. https://doi.org/10.1016/j.geoderma.2021.115590.
- Sanogo, K., Birhanu, B.Z., Sanogo, S., Ba, A., 2023. Landscape pattern analysis using gis and remote sensing to diagnose soil erosion and nutrient availability in two agroecological zones of southern mali. Agric. Food Secur. 12 (1), 4. https://doi.org/ 10.1186/s40066-023-00408-6.
- Schmidt, M., Wilson, R.E., Lee, S.S., Soderholm, L., Fenter, P., 2012. Adsorption of plutonium oxide nanoparticles. Langmuir 28 (5), 2620–2627. https://doi.org/ 10.1021/la2037247.
- Six, J., Elliott, E.T., Paustian, K., 2000. Soil macroaggregate turnover and microaggregate formation: A mechanism for c sequestration under no-tillage agriculture. Soil Biol. Biochem. 32 (14), 2099–2103.
- Stocking, M., 2014. Soil erosion and land degradation. In: O'Riordan, T. (Ed.), Environmental Science for Environmental Management. Routledge, pp. 287–321. https://doi.org/10.4324/9781315839592. Reprinted from 2nd.
- Tan, C., Cao, X., Yuan, S., Wang, W., Feng, Y., Qiao, B., 2015. Effects of long-term conservation tillage on soil nutrients in sloping fields in regions characterized by water and wind erosion. Sci. Rep. 5 (1), 17592. https://doi.org/10.1038/srep17592
- Tian, K., Li, M., Hu, W., Fan, Y. n, Huang, B., Zhao, Y., 2022. Environmental capacity of heavy metals in intensive agricultural soils: Insights from geochemical baselines and source apportionment. Sci. Total Environ. 819, 153078. https://doi.org/10.1016/j. scitotenv.2022.153078.
- Tsegaye, B., 2019. Effect of land use and land cover changes on soil erosion in ethiopia. Int. J. Agric. Sci. Food Technol. 5 (1), 026-034.

- Van Straaten, P., 2002. Rocks Crop. Agrominerals subSahar. Afr.
- VandenBygaart, A.J., Kroetsch, D., Gregorich, E.G., Lobb, D., 2012. Soil c erosion and burial in cropland. Glob. Change Biol. 18 (4), 1441–1452. https://doi.org/10.1111/i1365-2486.2011.02604.x
- Verheijen, F.G.A., Jones, R.J.A., Rickson, R.J., Smith, C.J., 2009. Tolerable versus actual soil erosion rates in europe. EarthSci. Rev. 94 (1), 23–38. https://doi.org/10.1016/j. earscirev.2009.02.003.
- Walling, D.E., 2013. The evolution of sediment source fingerprinting investigations in fluvial systems. J. Soils Sediment. 13 (10), 1658–1675. https://doi.org/10.1007/s11368-013-0767-2.
- Wang, L., Zhang, C., Peng, J., Xu, L., Wang, J., Cai, C., 2024. Splash erosion-induced soil aggregate turnover and associated organic carbon dynamics. Soil Tillage Res. 235, 105900. https://doi.org/10.1016/j.still.2023.105900.
- Wanyonyi, R.W., Mwangi, J.K., 2012. Impact of human population on land degradation in former Lugari district, Kakamega county, Kenya. Unpublished Master of Environmental Sciences Thesis. Kenyatta University, Nairobi.
- Watene, George, Yu, Lijun, Nie, Yueping, Zhu, Jianfeng, Ngigi, Thomas, Nambajimana, Dieu, J. d., Kenduiywo, & Benson. (2021). Water erosion risk assessment in the kenya great rift valley region. Sustainability, 13(2), 844. <a href="https://www.mdpi.com/2071-1050/13/2/844">https://www.mdpi.com/2071-1050/13/2/844</a>).
- Watts, M.J., Middleton, D.R., Marriott, A., Humphrey, O.S., Hamilton, E., McCormack, V., Menya, D., Farebrother, J., Osano, O.J.E., 2020. Iodine Status West. Kenya. A CommunityBased CrossSect. Surv. Urin. Drink. Water Iodine Conc. 42 (4), 1141–1151.
- Weidhuner, A., Hanauer, A., Krausz, R., Crittenden, S.J., Gage, K., Sadeghpour, A., 2021. Tillage impacts on soil aggregation and aggregate-associated carbon and nitrogen after 49 years. Soil Tillage Res. 208, 104878. https://doi.org/10.1016/j. still.2020.104878.
- Wiesmeier, M., Urbanski, L., Hobley, E., Lang, B., von Lützow, M., Marin-Spiotta, E., van Wesemael, B., Rabot, E., Ließ, M., Garcia-Franco, N., 2019. Soil organic carbon storage as a key function of soils-a review of drivers and indicators at various scales. Geoderma 333, 149–162.

- Xu, Y., Qiao, J., Hou, X., Pan, S., 2013. Plutonium in soils from northeast china and its potential application for evaluation of soil erosion. Sci. Rep. 3 (1), 3506. https://doi. org/10.1038/srep03506.
- Yan, M., Zhang, X., Liu, K., Lou, Y., Wang, Y., 2022. Particle size primarily shifts chemical composition of organic matter under long-term fertilization in paddy soil. Eur. J. Soil Sci. 73 (1), e13170. https://doi.org/10.1111/ejss.13170.
- Zhang, Y., Wang, Q., Mao, J., Zhou, B., Li, Y., Jiang, J., Duan, X., Zhong, R., 2024. Soil nutrient redistribution in sloping farmland of dry–hot valleys in the upper red river. CATENA 244, 108273. https://doi.org/10.1016/j.catena.2024.108273.
- Zhang, S., Zhang, X., Huffman, T., Liu, X., Yang, J., 2011. Influence of topography and land management on soil nutrients variability in northeast china. Nutr. Cycl. Agroecosystems 89 (3), 427–438. https://doi.org/10.1007/s10705-010-9406-0.
- Zhang, X.C., Zheng, F.L., Chen, J., Garbrecht, J.D., 2020. Characterizing detachment and transport processes of interrill soil erosion. Geoderma 376, 114549. https://doi.org/ 10.1016/j.geoderma.2020.114549.
- Zhao, Y., Li, Z., Cao, Z., Mi, W., Wang, H., 2023. Spatial patterns and drivers of soil total nitrogen in anthropogenic shrub encroachment in desert steppe [Original Research]. Front. Environ. Sci. 10. https://doi.org/10.3389/fenvs.2022.1058344.
- Zhao, P., Li, L., Lin, L., Zhai, G., Cruse, R.M., Wang, E., 2022. Response of surface soil nutrients and organic carbon fractions to tillage erosion vs. Water erosion in an agricultural landscape. Soil Sci. Soc. Am. J. 86 (6), 1470–1482. https://doi.org/10.1002/sai2.20461.
- Zhao, Y., Wang, H., Li, Z., Lin, G., Fu, J., Li, Z., Zhang, Z., Jiang, D., 2024. Anthropogenic shrub encroachment has accelerated the degradation of desert steppe soil over the past four decades. Sci. Total Environ. 946, 174487. https://doi.org/10.1016/j. scitotenv.2024.174487.
- Zheng, Y., Luo, X., Zhang, W., Wu, X., Zhang, J., Han, F., 2016. Transport mechanisms of soil-bound mercury in the erosion process during rainfall-runoff events. Environ. Pollut. 215, 10–17. https://doi.org/10.1016/j.envpol.2016.04.101.
- Zucca, C., Fleiner, R., Bonaiuti, E., Kang, U., 2022. Land degradation drivers of anthropogenic sand and dust storms. CATENA 219, 106575. https://doi.org/ 10.1016/j.catena.2022.106575.